Volume 24
Number 39
21 October 2022
Pages 23939–24596

PCCP

Physical Chemistry Chemical Physics

rsc.li/pccp

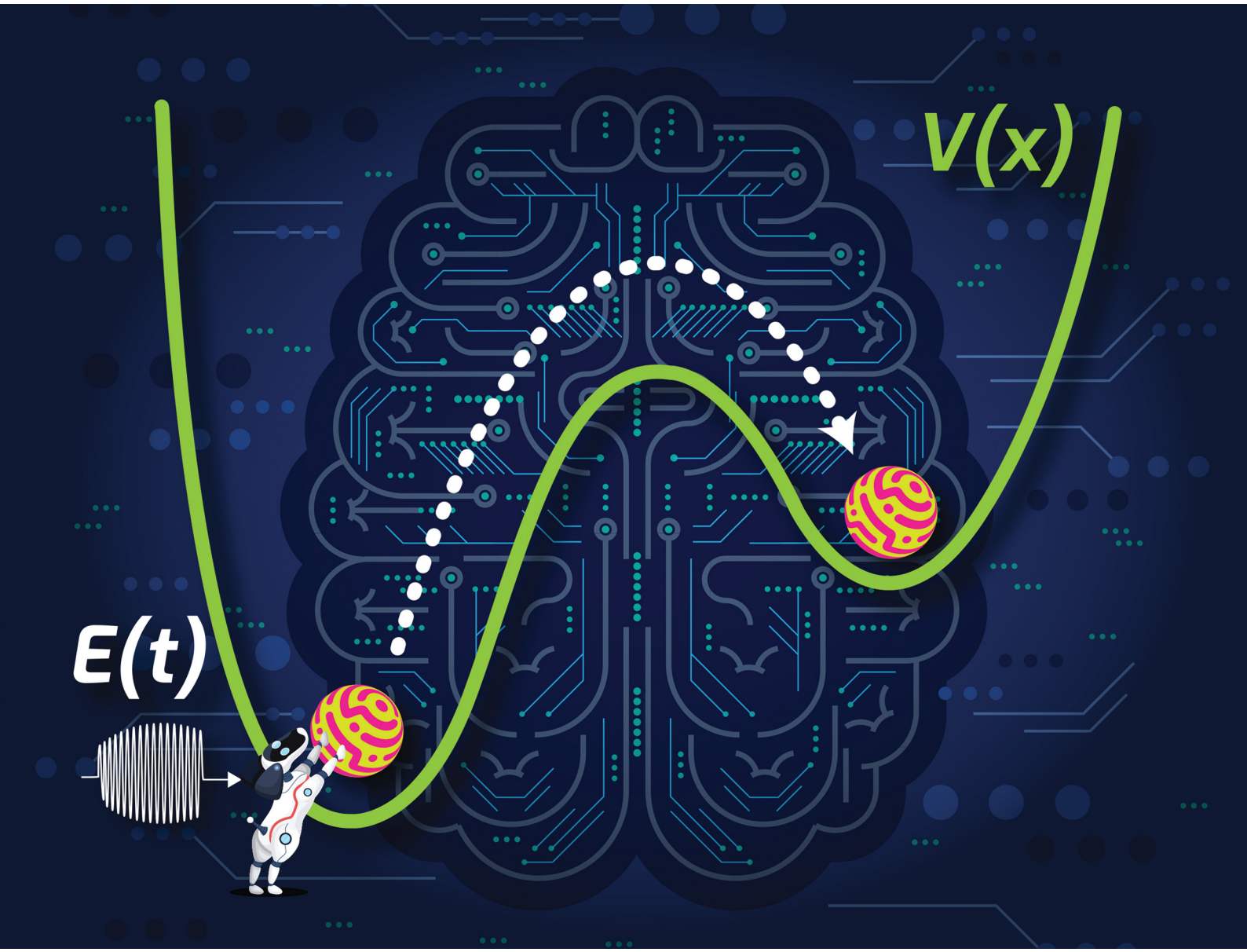

ISSN 1463-9076

ROYAL SOCIETY OF CHEMISTRY

PAPER

Nanpeng Yu, Bryan M. Wong *et al.*

Harnessing deep reinforcement learning to construct time-dependent optimal fields for quantum control dynamics

PCCP

ROYAL SOCIETY OF CHEMISTRY

PAPER

View Article Online
View Journal | View Issue

Cite this: *Phys. Chem. Chem. Phys.*, 2022, **24**, 24012

Harnessing deep reinforcement learning to construct time-dependent optimal fields for quantum control dynamics†

Yuanqi Gao, [a] Xian Wang, [b] Nanpeng Yu *[c] and Bryan M. Wong *[d]

Received 1st June 2022,
Accepted 9th September 2022

DOI: 10.1039/d2cp02495k

rsc.li/pccp

We present an efficient deep reinforcement learning (DRL) approach to automatically construct time-dependent optimal control fields that enable desired transitions in dynamical chemical systems. Our DRL approach gives impressive performance in constructing optimal control fields, even for cases that are difficult to converge with existing gradient-based approaches. We provide a detailed description of the algorithms and hyperparameters as well as performance metrics for our DRL-based approach. Our results demonstrate that DRL can be employed as an effective artificial intelligence approach to efficiently and autonomously design control fields in quantum dynamical chemical systems.

I Introduction

Inverse problems continue to garner immense interest, particularly in quantum control dynamics and quantum computing applications. In this context, quantum optimal control theory seeks to construct an external control field, $E(t)$, that evolves a quantum system from a known initial state to a target final state. Predicting the temporal form of $E(t)$ is essential for controlling the underlying dynamics in quantum computing,[1] quantum information processing,[2–4] laser cooling,[5,6] and ultracold physics.[7,8] In complex, many-body quantum systems, the prediction of optimal $E(t)$ fields provides critical initial conditions for controlling desired dynamical effects in light-harvesting complexes and many-body coherent systems.[9–13]

The conventional approach to solving these quantum control problems is to maximize the desired transition probability using either gradient-based methods or other numerically intensive methods.[14–17] Such approaches include the stochastic gradient descent over quantum trajectories,[18] the Krotov method,[19] the gradient ascent pulse engineering (GRAPE)[20] method, and the chopped random basis algorithm (CRAB)[21] approach. While each algorithm has its own purposes and advantages, the majority of these approaches require complex numerical methods to solve for the optimal control fields. Moreover, due to the nonlinear nature of these inverse problems, the number of iterations and floating point operations in these algorithms can be extremely large, sometimes even leading to unconverged results for relatively simple one-dimensional problems.[16,22]

To address the previously mentioned computational bottlenecks, our group recently explored the use of supervised machine learning to solve these complex, inverse problems in quantum dynamics.[23] In contrast to supervised machine learning, reinforcement learning (RL) techniques have attracted recent attention since these machine learning methods are designed to solve sequential decision-making tasks, which can be naturally suited for quantum control problems. However, all prior RL studies to date have focused on low-dimensional spin-1/2 systems, which generally require a relatively small number of control pulses (typically 10–100) to converge.[24–29] More specifically, the RL algorithms used in previous quantum control problems (such as tabular Q learning or policy gradient) assume a finite set of admissible control pulses and quantum state representations. While this is possible for finite-dimensional, spin-1/2 Hilbert spaces, they are typically ineffective for continuous (*i.e.*, chemical/material) Hamiltonian systems.

In this work, we develop an extremely efficient RL approach for solving chemical dynamics systems for the first time. Our RL formulation utilizes modern deep learning frameworks and has a computational performance that scales linearly with the control time horizon. We test our new machine learning approach against a wide range of quantum control benchmarks

[a] *Department of Electrical and Computer Engineering, University of California-Riverside, Riverside, CA, USA*
[b] *Department of Physics and Astronomy, University of California-Riverside, Riverside, CA, USA*
[c] *Department of Electrical and Computer Engineering, University of California-Riverside, Riverside, CA, USA. E-mail: nyu@ece.ucr.edu*
[d] *Department of Chemical and Environmental Engineering, Materials Science and Engineering Program, Department of Chemistry, and Department of Physics and Astronomy, University of California-Riverside, Riverside, CA, USA. E-mail: bryan.wong@ucr.edu*

† Electronic supplementary information (ESI) available. See DOI: https://doi.org/10.1039/d2cp02495k

to demonstrate that our RL approach significantly improves the fidelity and reduces the computation time compared to conventional gradient-based approaches. This paper is organized as follows: Section II reviews the background of quantum control in continuous systems and formulates it as a reinforcement learning problem. Section III presents the reinforcement learning techniques. Section IV provides the numerical results, and Section V concludes the paper with a discussion and future perspectives on prospective applications.

II Theory and problem formulation

We first discuss the basic theory and problem scope in three sequential subsections: Section A presents the quantum control problem, Section B briefly reviews the theory of Markov decision processes (MDPs), and Section C formulates the quantum control problem as an MDP. This problem formulation provides the necessary background to leverage deep reinforcement learning (DRL) algorithms for solving the quantum control problem for dynamical chemical systems.

A Brief overview of quantum control for chemical systems

Since the main purpose of this work is to harness reinforcement learning techniques for controlling dynamic chemical systems, we only give a brief overview of quantum optimal control and point the interested reader to several topical reviews in this area.[30–33] For chemical systems, the quantum optimal control formalism commences with the time-dependent Schrödinger equation for describing the temporal dynamics of nuclei, which, in atomic units is given by

$$i\frac{\partial}{\partial t}\psi(x,t) = \left[-\frac{1}{2m}\frac{\partial}{\partial x^2} + V(x) - \mu(x)E(t)\right]\psi(x,t) \qquad (1)$$

where x is the reduced coordinate along a chosen reaction path, m is the effective mass associated with the molecular motion along the reaction path,[34] $V(x)$ is the Born–Oppenheimer potential energy function/operator of the molecule, $\mu(x)$ is the dipole moment function, $E(t)$ is the time-dependent external electric field, and $\psi(x,t)$ is the wavefunction for the motion of the nuclei along the reduced coordinate path. Both $V(x)$ and $\mu(x)$ can be obtained from a quantum chemistry calculation by carrying out a potential energy scan.[35–37]

With the time-dependent Schrödinger equation defined in eqn (1), the quantum control problem can be stated as follows: given a starting state $\psi_0(x)$ and a desired final state $\psi_f(x)$, what is the temporal form of the electric field $E(t)$, $t \in (0,T)$ that propagates the state $\psi_0(x)$ to $\psi_f(x)$? In other words, the quantum control formalism seeks the electric field that maximizes the following functional:

$$J[\psi, E] = \left|\int_{-\infty}^{\infty} \psi_f^*(x)\psi(x, t=T)\mathrm{d}x\right|^2, \qquad (2)$$

where $\psi_f(x)$ is a desired target final wavefunction given by the user, and $\psi(x,t = T)$ is obtained by propagating $\psi_0(x)$ in time (*via* the time-dependent Schrödinger equation) to $t = T$. In short, eqn (2) measures the similarity (fidelity) between the target and actual wavefunction at time T.

In this work, we harness new RL techniques to automatically construct optimal control fields, $E(t)$, that enable desired transitions in these dynamical systems. To test the performance of our RL approach, we compare against the NIC-CAGE (Novel Implementation of Constrained Calculations for Automated Generation of Excitations) code,[38] which solves the quantum control problem using a traditional gradient-based approach. Specifically, the NIC-CAGE code utilizes analytic gradients based on a Crank–Nicolson propagator, which are computationally more efficient than other matrix exponential approaches (such as those used in the GRAPE[39] or QuTIP[40,41] packages) or higher-order time-propagation methods.[42] As such, a comparison against the execution times of the already optimized NIC-CAGE code serves as an excellent benchmark test of the performance of our RL methods. Before describing our reinforcement learning approach, we first provide a brief review of Markov decision processes (MDPs) in the next section.

B Review of Markov decision processes (MDPs)

MDPs[43] are a class of mathematical formulations for sequential decision-making problems. In an MDP, we define a state space $\mathcal{S}$, an action space $\mathcal{A}$, a state transition probability $P(s'|s,a)$, and a reward function $r(s,a)$. At each time step t, the state of the "environment" is represented by an element $s_t \in \mathcal{S}$. A learning "agent" can interact with this environment by taking some action $a_t \in \mathcal{A}$ based on s_t. The environment provides a reward $r_{t+1} = r(s_t,a_t)$ to the agent and transitions to other states s_{t+1} according to the state transition probability function $s_{t+1} = P(\cdot|s_t,a_t)$. The above process repeats iteratively. Given the current state s_t and action a_t, the state transition function dictates that the next state s_{t+1} is conditionally independent of all previous state and actions.

The goal of the learning agent is to find a policy $\pi(a|s)$, which is a rule for taking actions based on states, such that the expected discounted return $v^\pi(s)$ is maximized:

$$v^\pi(s) := \mathbb{E}_\pi\left[\sum_{t=0}^{T}\gamma^t r_{t+1}|s_0 = s\right], \qquad (3)$$

$$v^*(s) = \max_\pi v^\pi(s) \quad \forall s. \qquad (4)$$

The notation $\mathbb{E}_\pi[\cdot|s_0 = s]$ denotes the expectation of the quantity $\cdot$ starting from a state s, which then follows the policy π thereafter. The constant $\gamma < 1$ controls the contribution of future rewards to the optimizing objective, and T is the optimization horizon which may be infinite. Note that the policy $\pi(a|s)$ is a probability distribution over $\mathcal{A}$ conditioned on an $s \in \mathcal{S}$. The agent takes action by sampling an element from the distribution $a_t = \pi(\cdot|s_t)$.

Another function commonly used in reinforcement learning is the action-value function defined as

$$q^\pi(s,a) = \mathbb{E}_\pi\left[\sum_{t=0}^{T}\gamma^t r_{t+1}|s_0 = s, a_0 = a\right], \qquad (5)$$

$$q^*(s,a) = \max_{\pi} q^{\pi}(s,a) \quad \forall s,a. \tag{6}$$

With these quantities properly defined, we formulate the quantum control problem as an MDP in the next section.

C Formulating quantum control as an MDP

To formulate the quantum control problem as an MDP, we must define the time variable, state, action, and reward:

Time variable. The time variable, t, of the MDP is naturally defined as the time in the quantum control problem, which we discretize into evenly spaced intervals of duration τ.

State. The state at time step t is defined as $s_t = [P_t^0, P_t^1, \ldots, P_t^K, g_t]$. P_t^k, $k = 0, \ldots, K$ is the squared magnitude of the projection of the current wavefunction, $\psi(x,t)$, onto the kth eigenstate, $\psi^k(x)$, of the time-independent Schrödinger equation:

$$P_t^k = \left| \int_{-\infty}^{\infty} \psi^*(x,t)\psi^k(x)\mathrm{d}x \right|^2 \tag{7}$$

We include the various P_t^k terms in our state space since it gives additional information to the reinforcement learning agent about the current wavefunction. The variable K is a design parameter that is described further in Section IV. The variable g_t is the gradient of the fidelity with respect to the electric field, E, evaluated at $E(t-1)$:

$$g_t = \left. \frac{\partial P_t^k}{\partial E} \right|_{E=E(t-1)}. \tag{8}$$

To calculate this gradient, we re-express P_t^k as

$$\begin{aligned} P_t^k &= \left| \int_{-\infty}^{\infty} \psi^*(x,t)\psi^k(x)\mathrm{d}x \right|^2 \\ &= \left| \int_{-\infty}^{\infty} \mathcal{F}(\psi(x,t-1), E(t-1))^* \psi^k(x)\mathrm{d}x \right|^2, \end{aligned} \tag{9}$$

where $\mathcal{F}(\psi, E)$ is an algorithm that performs one propagation step of the wavefunction (*i.e.*, $\mathcal{F}(\psi, E)$ propagates one step of the time-dependent Schrödinger equation in eqn (1)). We approximate the integral in eqn (9) with a finely-spaced Riemann sum and leverage the auto-differentiation engine from the PyTorch deep learning framework[44] to calculate the gradient. Adding this gradient information provides the machine learning agent with the direction in which the fidelity can possibly be improved.

Action. The action at time step t is defined as the amplitude of the electric field $a_t = E(t)$, where the minimum and maximum amplitude is restricted to $E_{\min}$ and $E_{\max}$, respectively.

Reward. The reward to the agent after taking an action a_t is defined as $r_{t+1} = P_{t+1}^{\kappa}$ (*i.e.*, the immediate next fidelity score).

This brief explanation completes the formulation of quantum control as a reinforcement learning problem. In the next section, we provide the technical details for utilizing RL to solve our quantum control problem in reduced-dimensional chemical systems.

III Deep reinforcement learning for predicting optimal electric fields

In this section, we describe our DRL approach for solving the MDP problem. An overview of our framework is illustrated in Fig. 1, which shows the MDP formulation, RL algorithm, and the interaction between the two. In the next subsection, we give further details on the theory and algorithms used in our reinforcement learning agent.

A Overview of reinforcement learning

Reinforcement learning (RL) algorithms autonomously estimate the optimal policy $\pi^\star$ by interacting with a given environment. It is well-known that under mild technical assumptions, a deterministic stationary optimal policy exists,[45] which is given by:

$$\pi^*(\cdot|s) = \operatorname*{argmax}_a q^*(s,a). \tag{10}$$

In an optimal policy, the expected discounted return from state s equals $v^\star(s)$, the optimal state value of s. In other words, $v^*(s) = \max_a q^*(s,a)$. The relationship in eqn (10) reveals that estimating $\pi^*(a|s)$ or $q^*(s,a)$, or both at the same time are equally useful in solving MDP problems. As such, RL algorithms can be classified as policy gradient methods (estimating $\pi^\star$), action-value methods (estimating $q^\star$), and actor-critic methods (estimating both $\pi^\star$ and $q^\star$). For MDPs with a finite state and action space, the policy and value functions can be maintained in a table. However, our particular quantum control problem has

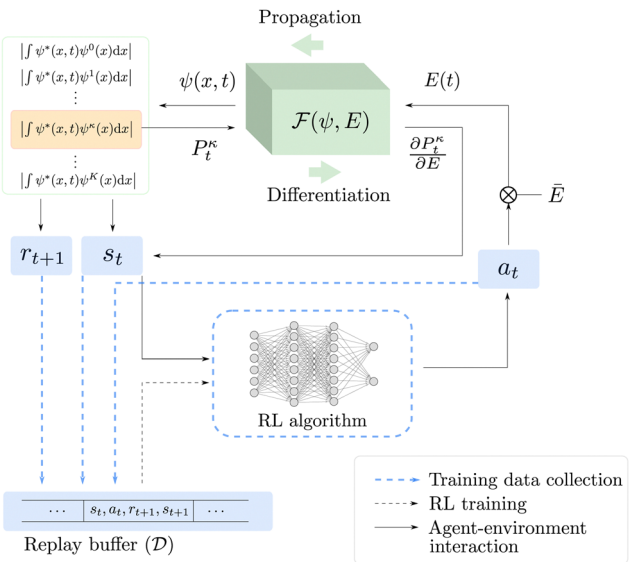

Fig. 1 RL-based QOC framework utilized in this work. Solid lines represent the interactions between the RL algorithm and the time-dependent Schrödinger equation, blue dashed lines represent the training data collection, and black dashed lines represent the training of the RL algorithm. At each time step t, the RL algorithm outputs an action a_t based on the state s_t, and a_t is then converted to an electric field $E(t)$. The time-dependent Schrödinger equation block performs a forward propagation and a backward differentiation to obtain the next state s_{t+1} and reward r_{t+1}. The tuple s_t, a_t, r_{t+1}, and s_{t+1} is stored in the replay buffer $\mathcal{D}$.

a continuous state space that must be represented by function approximators such as neural networks.

To learn the optimal policy, RL algorithms must properly balance the conflicting objectives of exploring the state-action space as much as possible to collect environment feedback, while only visiting useful portions to act optimally. This is known as the exploration–exploitation trade-off. In the terminology of quantum control, the RL algorithm must explore different external electric fields, $E(t)$, before it recognizes the optimal one. However, to be efficient, this exploration should not take too long since it may undermine computational performance. We briefly review two of the popular methods to balance exploration and exploitation in our work.

Epsilon greedy. The Epsilon greedy[46] algorithm explores the state-action space by following the optimal policy, while occasionally taking a random action uniformly sampled from the action space:

$$a_t = \begin{cases} \underset{a}{\operatorname{argmax}}\, q(s_t, a) & \xi > \varepsilon \\ a_t = \mathcal{U}(\mathcal{A}) & \xi \leq \varepsilon \end{cases} \tag{11}$$

where $\xi = \mathcal{U}(0,1)$ is a uniform distribution between 0 and 1, and ε is a constant between 0 and 1. In practice, ε may start with a large value and becomes gradually annealed as the training progresses.

Entropy bonus. In the maximum entropy RL framework,[47] the entropy of the policy $H(\pi(\cdot|s)) = -\int \pi(a|s)\log\pi(a|s)\mathrm{d}a$ is added to the reward to maintain high stochasticity of the policy when the collected reward value is small:

$$r^{\mathrm{h}}(s,a) = r(s,a) + \alpha H(\pi(\cdot|s)), \tag{12}$$

where α is the temperature parameter that controls the influence of the entropy to the reward. Policies learned from $r^{\mathrm{h}}(s,a)$ tend to have a higher stochasticity than the ones learned from $r(s,a)$ alone. Therefore, the sampled actions $a_t = \pi(\cdot|s)$ have a higher chance of visiting a larger portion of the state-action space.

In our work, two DRL algorithms are harnessed to solve the quantum control problem: deep Q learning and soft actor-critic, both of which are described below.

B Deep Q learning

Deep Q learning[46] is a value-based algorithm that uses deep neural networks to learn the optimal value function $q^*(s,a)$. A neural network $q_\theta(s,a)$ was used to approximate the optimal value function as follows:

$$J(\theta) = \frac{1}{B}\sum_{(s,a,r,s')\in\mathcal{B}}\left(r + \gamma \max_{a'} q_{\theta^-}(s',a') - q_\theta(s,a)\right)^2, \tag{13}$$

$$\theta \leftarrow \theta - \delta\nabla J(\theta), \tag{14}$$

where $\mathcal{B}$ is a mini-batch randomly sampled from the experience replay buffer $\mathcal{D}$. The latter maintains a fixed number of the most recent agent-environment interaction data, $B = |\mathcal{B}|$ is the mini-batch size, $q_{\theta^-}(s,a)$ is another neural network with an identical architecture as q_θ, and δ is the learning rate. The parameters θ^- are copied from θ after every few iterations to stabilize the training. Since finding the maximum for the Q network over the action space is intractable, the deep Q learning algorithm may only be used for finite and discrete action space MDPs. Discretization is commonly used when the action is continuous, and the epsilon greedy algorithm is typically used in conjunction with deep Q learning. In our MDP formulation of the quantum control problem, the neural network $q_\theta(s_t,a)$ is interpreted as the discounted cumulative fidelity score calculated from $\sum_{\tau=t}\gamma^\tau P_\tau^K$ at time t, and the electric field is set to $E(t) = a$. Therefore, the optimal electric field at time t is $a^* = \underset{a}{\operatorname{argmax}}\, q_\theta(s_t, a)$.

In this paper, we adopt two important extensions to the basic deep Q learning algorithm, namely, the dueling architecture[48] and the double deep Q learning,[49] which have achieved improved performance on other control benchmarks. The dueling architecture decomposes the Q value estimate into a state value and advantage function estimate according to the formula $q^\pi(s,a) = v^\pi(s) + A^\pi(s,a)$. As a result, the dueling Q network replaces the output of the standard neural network, $q_\theta(s,a)$, with two intermediate output streams: $v_{\theta,\beta}(s)$ and $A_{\theta,\alpha}(s,a)$. The final output, which is the Q value estimate, is given by the following aggregation of the two intermediate streams:

$$q_\Theta(s,a) = v_{\theta,\theta_{\mathrm{V}}}(s) + \left(A_{\theta,\theta_{\mathrm{A}}}(s,a) - \frac{1}{|\mathcal{A}|}\sum_u A_{\theta,\theta_{\mathrm{A}}}(s,u)\right). \tag{15}$$

We use the symbol $\Theta = (\theta,\theta_{\mathrm{A}},\theta_{\mathrm{V}})$ to collectively "absorb" all parameters of the hidden layers and the two output streams. Subtracting the average of $A_{\theta,\alpha}$ on the right-hand side of eqn (15) resolves the lack of identifiability of the value-advantage decomposition. The dueling architecture allows the value function to be learned more efficiently.

The double deep Q learning network (DDQN) approach modifies the loss function in eqn (13) as:

$$\begin{aligned} J^d(\Theta) &= \frac{1}{B}\sum_{(s,a,r,s')\in\mathcal{B}}\left(r + \gamma q_{\Theta^-}(s', a') - q_\Theta(s,a)\right)^2 \\ a' &= \underset{u}{\operatorname{argmax}}\, q_\Theta(s', u) \end{aligned} \tag{16}$$

Compared with eqn (13), eqn (16) decomposes the max operator into a separate action selection and evaluation procedure. This mitigates the overestimation issue with the max operator in eqn (13) and leads to a more consistent estimation.

C Soft actor-critic

The soft actor-critic (SAC)[47] approach is an actor-critic algorithm developed recently using the maximum entropy framework. The algorithm trains deep neural network-parameterized policy and value functions, $\pi_\phi(a|s)$ and $q_\theta(s,a)$, to approximate the optimal maximum entropy policy and value functions, respectively. $\pi_\phi(a|s)$ is a neural network that takes s as the input and outputs a probability distribution over the action space $\mathcal{A}$. For mathematical tractability purposes, this probability distribution is often chosen

as the tanh-squashed Gaussian:

$$\xi_t = \mathcal{N}(u; 0, 1), \tag{17}$$

$$u_t = \xi_t \cdot \sigma_\phi(s_t) + \mu_\phi(s_t), \tag{18}$$

$$a_t = \tanh(u_t). \tag{19}$$

That is, the neural network outputs the mean $\mu_\phi(s)$ and standard deviation $\sigma_\phi(s)$ of the action for a given state s, where the distribution is defined by $\pi_\phi(a|s) = \tanh(a_\phi)$ and $a_\phi = \mathcal{N}(a; \mu_\phi(s), \sigma_\phi(s))$. The tanh function squeezes the Gaussian variable into a finite range and ensures a bounded action. In the context of the quantum control problem, eqn (17)–(19) states that the external electric field, $E(t)$, at time t generated by the SAC algorithm is a Gaussian random variable, whose mean and variance is given by some learned neural network. The variance is maintained to ensure a sufficient exploration of $E(t)$. The action-value function network, $q_\theta(s,a)$, takes the (s,a) pair as input and outputs a single number to represent the action value.The SAC algorithm additionally employs the target neural network $q_{\theta^-}(s,a)$, similar to the deep Q learning algorithm. Also, two action-value networks are maintained instead of one to stabilize the training. As a result, four neural networks are responsible for the estimation of the following functions: $q_{\theta^1}(s,a)$, $q_{\theta^2}(s,a)$, $q_{\theta^{1-}}(s,a)$, and $q_{\theta^{2-}}(s,a)$.

The training of the policy neural network, $\pi_\phi(a|s)$, and value networks, $q_{\theta^i}(s,a)$ for $i = 1, 2$, are carried out as follows. At each iteration, the policy neural network is trained to minimize the temporal difference error $J(\theta^i)$:

$$J(\theta^i) = \frac{1}{B} \sum_{(s,a,r,s') \in \mathcal{B}} \Big(q_{\theta^i}(s,a) - r + \gamma \Big(\min_{i \in \{1,2\}} q_{\theta^{i-}}(s', a') - \alpha \log \pi_\theta(\tilde{a}'|s') \Big) \Big)^2 \tag{20}$$

$$\theta^i \leftarrow \theta^i - \delta \nabla J(\theta^i) \quad i = 1, 2, \tag{21}$$

where $\tilde{a}' = \pi_\phi(a|s')$ is a random sample from the current policy. The policy neural network is trained using the following gradient ascent approach:

$$J(\phi) = \frac{1}{B} \sum_{(s,a,r,s') \in \mathcal{B}} \min_{i \in \{1,2\}} q_{\theta^i}(s, a_\phi) - \alpha \log \pi_\phi(a_\phi|s), \tag{22}$$

$$\phi \leftarrow \phi + \delta \nabla J(\phi), \tag{23}$$

where $a_\phi = \pi_\phi(a|s)$ is a random sample from the current policy. Finally, the target network is updated using the exponential moving average:

$$\theta^{i-} \leftarrow \rho \theta^{i-} + (1 - \rho)\theta^i \quad i = 1, 2. \tag{24}$$

D Summary of our RL algorithm for quantum control

Our RL-based quantum control framework is summarized in the Algorithm 1 flowchart. For conciseness, we have summarized the deep Q learning and SAC approaches in the same pseudocode (they differ by Lines 3 and 8). More detailed descriptions of our implementation of these algorithms are given in the ESI.†

Algorithm 1 RL for QOC

1: Initialize neural network weights and s_0
2: **for** $t = 0, \ldots,$ **do**
3: Sample $a_t = \pi(\cdot|s_t)$. The sampling is defined by eqn (11) for deep Q learning and eqn (17)–(19) for SAC
4: $E(t) \leftarrow a_t \cdot \bar{E}$
5: Perform one environment step to obtain s_{t+1}, r_{t+1} according to Section II A
6: Store $(s_t, a_t, r_{t+1}, s_{t+1})$ into the replay buffer $\mathcal{D}$
7: Sample mini-batch $\mathcal{B} = \{(s, a, r, s')\}$ from $\mathcal{D}$
8: Train the RL algorithm by performing eqn (16) for deep Q learning and eqn (20)–(24) for SAC
9: **if** $P_t^\kappa > \bar{P}$ **then**
10: Break

At each time step t, the agent takes an action, a_t, according to the state s_t and converts it to an electric field $E(t) = a_t\bar{E}$, where $\bar{E}$ is the upper/lower limit of the magnitude of the electric field. The environment then transitions to the next state according to the Markov decision process defined in Section II C. The agent-environment interaction transition $(s_t, a_t, r_{t+1}, s_{t+1})$ is stored in the replay buffer. Tuples of this form will be randomly sampled to train the neural networks of the deep Q learning and SAC algorithm. The procedure stops when the fidelity P_t^κ is above a pre-defined threshold $\bar{P}$, which we set to 0.99 in this work.

IV Results

In this section, we compare the performance of the various RL algorithms against the gradient-based approach from the NIC-CAGE algorithm. Section IV A describes the algorithm and hardware setup used in this work. Section IV B reports the performance of RL compared to the NIC-CAGE benchmarks, and Section IV C concludes with a discussion of a particularly difficult case.

A Numerical setup

Similar to our previous work on quantum control of molecular systems,[23] we generated a set of potentials $\{V_i(x)\}_{i=1,2,\ldots}$ of the form:

$$V_i(x) = -\sum_{k=1}^{3} A_{i,k} \exp\left(-\frac{(x - \mu_{i,k})^2}{2\sigma_{i,k}{}^2} \right), \tag{25}$$

where $A_{i,k} = \mathcal{U}(1, 10)$, $\mu_{i,k} = \mathcal{U}(-3, 3)$, and $\sigma_{i,k} = \mathcal{U}(0.5, 2)$, and $\mathcal{U}$ denotes a uniform distribution. A comprehensive listing of the parameters used to generate the various potentials, $V_i(x)$, in this work can be found in the ESI.† The functional form of these potentials mimic a bond stretching or dissociation

Table 1 Hyperparameters used in our RL algorithms

	SAC	DDQN
Hidden layers	(200, 200)	(200, 200)
Hidden activation	ReLu	ReLu
Discount factor (γ)	0.99	0.99
Minibatch size	64	64
Optimizer	Adam	Adam
Learning rate	0.0003	0.0001
Electric field bound ($\bar{E}$)	0.2	0.1
Temperature parameter (α)	0.1	—
Smoothing coefficient (ρ)	0.005	—
Target updating frequency	—	100
Epsilon max	—	0.5
Epsilon min	—	0.01
Epsilon annealing	—	$\frac{1}{3}$ of training
Action discretization	—	15

process in a photo-induced reaction. The range of x is restricted to the interval $[-8,8]$ and discretized into 192 equally-spaced intervals. The entire time duration T is also discretized into intervals of length 0.1. The range of the electric field amplitude is constrained to lie within the $[-0.9,0.9]$ interval. The total number of states used to define the state space for our RL algorithms is set to 5 (or $K = 4$ in the notation of Section II). The dipole moment function $\mu(x)$ in eqn (1) was set to x.

Algorithm setup. The hyperparameters for our RL algorithm are provided in Table 1, which we manually tuned on 10 selected potentials. Nevertheless, we found that the algorithm's performance was insensitive to small variations for most of the hyperparameters. Unless specified otherwise, these values were used for all of our subsequent simulations.

Hardware/software setup. The NIC-CAGE package is implemented in Python with the NumPy and SciPy package; the one-step forward propagation of the Schrödinger equation and the RL algorithms are implemented in Python with the PyTorch deep learning framework. All simulations were executed on the Extreme Science and Engineering Discovery Environment (XSEDE) Comet computing cluster at the University of California, San Diego. To provide a fair comparison between the NIC-CAGE and RL approaches examined in this work, each computation utilized 2 Intel Xeon E5 cores.

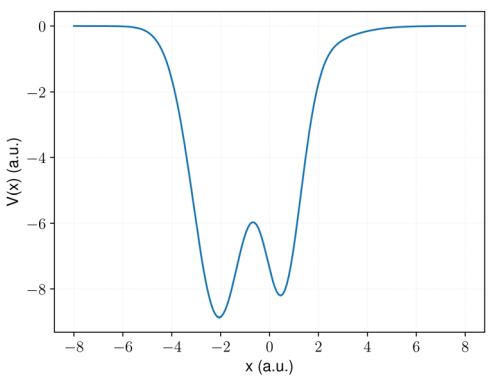

Fig. 2 Example of a potential with a small effective mass used in this work.

B Fidelity and computation time

For illustrative purposes, we commence with a relatively easy case for a potential with a small effective mass ($m = 1.0$) (Fig. 2) to understand the performance of the RL and NIC-CAGE approaches.

The converged electric field and fidelity, as well as the power spectrum of the electric field for all methods are shown in Fig. 3a–c.

All of the ML algorithms examined in this work automatically construct an electric field that propagates the initial state to the desired target state with a fidelity larger than 0.99. However, the difference is that the NIC-CAGE algorithm concurrently updates the electric field for all time steps in each iteration, whereas the RL algorithms developed in this paper sequentially add a new electric field data point at each time step (*i.e.*, the RL "learns" the electric field in an automated fashion). Fig. 3d plots the power spectrum for each of the electric fields shown in Fig. 3a–c. Interestingly, the NIC-CAGE and SAC algorithms produce relatively smooth electric fields and power spectra, whereas the DDQN approach employs an action-discretization approach, resulting in an electric field and power spectrum with significant noise. As such, the SAC algorithm can be used to improve other RL methods, such as those used to construct optimal fields for spin-1/2 systems in quantum computing. The control fields obtained in these prior studies are typically not smooth,[26] making them difficult to realize in experiments, whereas the SAC algorithm used here can ameliorate these artifacts.

When the effective mass is set to a larger value of $m = 10.0$, computing the optimal electric field becomes significantly more difficult. Large masses pose significant difficulties since they correspond to quantum optimal control of macroscopic objects (for example, quantum mechanical tunneling through a

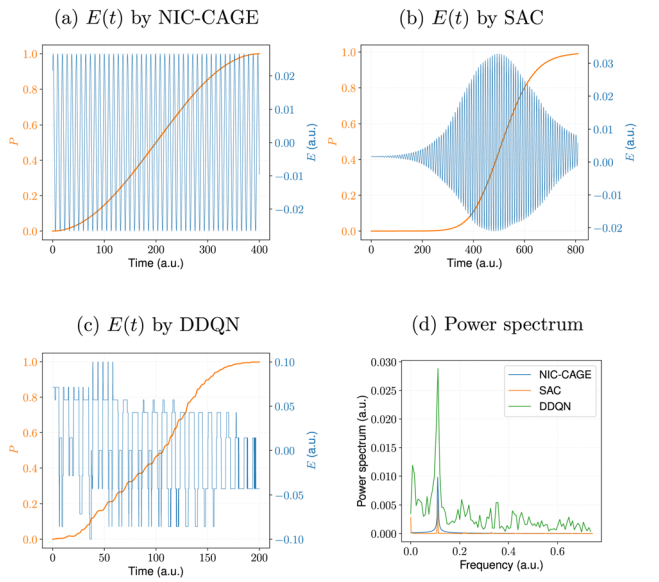

Fig. 3 Electric fields, $E(t)$, computed by the (a) NIC-CAGE algorithm and various reinforcement learning algorithms: (b) SAC and (c) DDQN. The power spectrum for all cases is shown in panel (d).

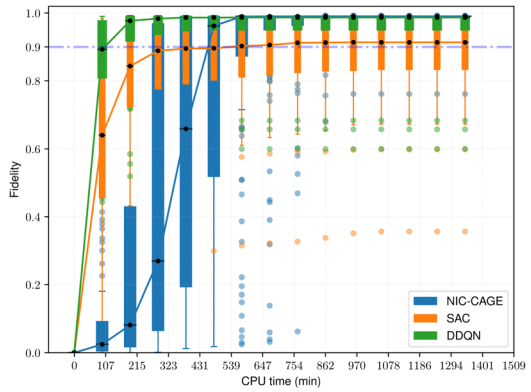

Fig. 4 Performance comparison between RL and NIC-CAGE on easy cases.

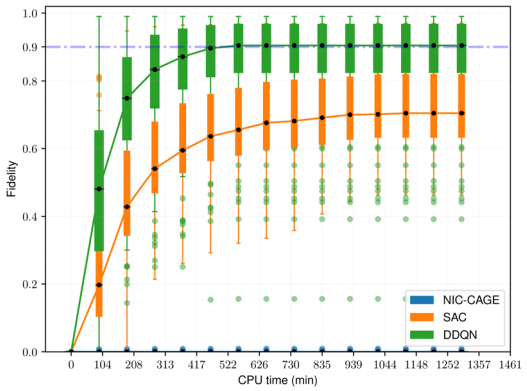

Fig. 6 Performance comparison between RL and NIC-CAGE on hard cases.

potential energy barrier is significantly more difficult for a larger mass than a smaller one). For some potentials, the NIC-CAGE algorithm does not converge to a high-fidelity solution within a reasonable computation time. To further compare the performance of the various RL algorithms against the traditional NIC-CAGE approach, we classified all the potentials into three groups based on the range of fidelities obtained by the NIC-CAGE algorithm: [0.75,1.0] designates easy cases, [0.01,0.75) are medium-difficulty cases, and [0.0,0.01) are hard cases. There are 89, 47, and 149 potentials in each group, respectively.

The fidelity *vs.* computation time for all methods is shown in Fig. 4–6. For the easy cases, the NIC-CAGE benchmark converges to high-fidelity solutions but requires long computation times. In contrast, the DDQN algorithm gives a similar fidelity as the NIC-CAGE benchmarks but with less computational effort. The SAC algorithm is only slightly worse than the DDQN method. Examining the medium-difficulty and hard cases (which account for $\sim$66% of all the tested potentials), we find that both DDQN and SAC significantly improve on the fidelity compared to the gradient-based NIC-CAGE approach. In particular, both RL methods are significantly more effective in scenarios where the NIC-CAGE algorithm only gives a low-fidelity solution, as shown by the hard cases in Fig. 6. It is worth noting that the quantum control problem for some potentials can be difficult to converge with RL, as shown by the outliers in each of the bar plots. We discuss these special cases in the next subsection and demonstrate that increasing the computation time improves their fidelity for RL (whereas these cases still remain unsolvable with the gradient-based NIC-CAGE algorithm).

As shown in Fig. 4–6, DDQN generally produces better results than the SAC method. In the context of machine learning, we carried out an ablation study to show which extension contributes the most to its superior performance. Table 2 shows the fidelity for all cases across Fig. 4–6 arranged in the 10, 50, and 90 percentiles. Each row is a variant of deep Q learning: basic DQN, double DQN, DQN with dueling architecture, and double DQN with dueling architecture. In particular, We found that both extensions improved the performance of DQN, when used alone or combined.

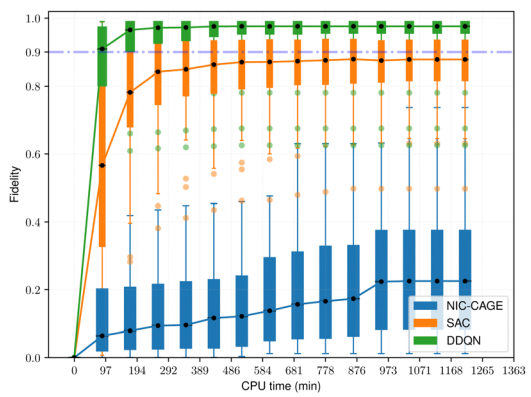

Fig. 5 Performance comparison between RL and NIC-CAGE on medium-difficulty cases.

C Case study: double-well potentials and large effective masses

As mentioned in Section IV B, although our RL algorithms generally outperform the gradient-based NIC-CAGE benchmarks, a few outlier potentials can be challenging to converge with RL. One such example is shown in Fig. 7a, which has a complex "double well" shape. These double-well potentials pose significant challenges since they correspond to quantum mechanical tunneling processes through a large potential barrier. The optimal electric fields that enable these unique transitions are typically quite complex. As such, for this potential, the gradient-based NIC-CAGE algorithm dramatically fails to converge (with $P < 10^{-28}$) even after five hours of computation. However, our DDQN method reaches a much

Table 2 Average performance of DQN and its extensions for easy, medium, and hard cases

	Easy	Medium	Hard	All
DQN	0.931	0.927	0.833	0.879
Double DQN	0.957	0.949	0.847	0.898
Dueling DQN	0.958	0.958	0.836	0.894
Dueling + double	0.961	0.949	0.862	0.907

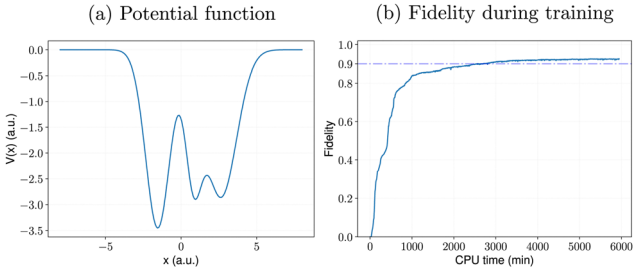

Fig. 7 Learning performance of RL for (a) a potential that is difficult to solve with gradient-based quantum control methods. For this particular case, the NIC-CAGE algorithm fails to converge (with a transition probability of $P < 10^{-28}$) after five hours of computation. In contrast, the DDQN-based reinforcement learning approach gives a higher fidelity and continues to improve as the algorithm runs longer, as shown in panel (b).

higher fidelity within the same computation time. Most importantly, our DDQN approach eventually reaches a 0.9 fidelity after about 3000 minutes of computation, which is not possible with the NIC-CAGE code. Most importantly, Fig. 7b plots the fidelity during the training, which shows that our RL approach can solve these quantum control problems that are not possible with the gradient-based NIC-CAGE algorithm.

V Conclusion

In conclusion, we have presented a new reinforcement learning framework for accurately and efficiently solving quantum optimal control problems for dynamical chemical systems. Our approach is formulated as a Markov decision process that leverages RL to autonomously construct electric fields that enable desired transitions in these quantum chemical systems. To test the performance of these techniques, we carried out extensive numerical studies showing that RL produces high fidelity solutions significantly faster than numerically-optimized gradient-based approaches. Regarding the advantages/disadvantages of the RL algorithms explored in this work, DDQN is preferred over SAC if the system under study can accept discrete/non-smooth values of $E(t)$ (the DDQN algorithm is easier to implement and requires less computation per training iteration). However, if discrete values of $E(t)$ are not realizable/acceptable, DDQN cannot be directly implemented, and SAC should be used since it can generate continuous and smooth optimal control fields. Most importantly, we show that both RL approaches can significantly improve the fidelity in quantum control problems that are difficult (or even impossible) to solve with gradient-based methods.

Looking forward, we anticipate that the RL techniques in this work could be used as efficient (and sometimes superior) alternatives to gradient-based approaches in quantum control problems. In particular, our RL approaches are expected to be even more efficient in high-dimensional quantum systems or applications with a large number of qubits. For both of these examples, calculations of the high-dimensional gradients would be computationally expensive, whereas the RL approach (which does not require these gradients) would be significantly more efficient. As such, these new RL techniques could be a viable option for obtaining optimal control fields of large quantum systems where gradient-based calculations are intractable or prohibitively out of reach.

Conflicts of interest

There are no conflicts to declare.

Acknowledgements

This work was supported by the U.S. Department of Energy, Office of Science, Office of Advanced Scientific Computing Research, Scientific Discovery through Advanced Computing (SciDAC) program under Award Number DE-SC0022209. This work used the Extreme Science and Engineering Discovery Environment (XSEDE) Comet computing cluster at the University of California, San Diego, through allocation TG-ENG160024.

References

1 D. Castaldo, M. Rosa and S. Corni, *Phys. Rev. A*, 2021, **103**, 022613.
2 K. C. Nowack, F. H. L. Koppens, Y. V. Nazarov and L. M. K. Vandersypen, *Science*, 2007, **318**, 1430–1433.
3 M. Kues, C. Reimer, P. Roztocki, L. R. Cortés, S. Sciara, B. Wetzel, Y. Zhang, A. Cino, S. T. Chu, B. E. Little, D. J. Moss, L. Caspani, J. Azaña and R. Morandotti, *Nature*, 2017, **546**, 622–626.
4 E. M. Fortunato, M. A. Pravia, N. Boulant, G. Teklemariam, T. F. Havel and D. G. Cory, *J. Chem. Phys.*, 2002, **116**, 7599–7606.
5 H. J. Williams, L. Caldwell, N. J. Fitch, S. Truppe, J. Rodewald, E. A. Hinds, B. E. Sauer and M. R. Tarbutt, *Phys. Rev. Lett.*, 2018, **120**, 163201.
6 A. Bartana, R. Kosloff and D. J. Tannor, *Chem. Phys.*, 2001, **267**, 195–207.
7 B. L. Brown, A. J. Dicks and I. A. Walmsley, *Phys. Rev. Lett.*, 2006, **96**, 173002.
8 M. J. Wright, J. A. Pechkis, J. L. Carini, S. Kallush, R. Kosloff and P. L. Gould, *Phys. Rev. A: At., Mol., Opt. Phys.*, 2007, **75**, 051401.
9 M. B. Oviedo and B. M. Wong, *J. Chem. Theory Comput.*, 2016, **12**, 1862–1871.
10 N. V. Ilawe, M. B. Oviedo and B. M. Wong, *J. Chem. Theory Comput.*, 2017, **13**, 3442–3454.
11 N. V. Ilawe, M. B. Oviedo and B. M. Wong, *J. Mater. Chem. C*, 2018, **6**, 5857–5864.
12 M. Maiuri, M. B. Oviedo, J. C. Dean, M. Bishop, B. Kudisch, Z. S. D. Toa, B. M. Wong, S. A. McGill and G. D. Scholes, *J. Phys. Chem. Lett.*, 2018, **9**, 5548–5554.
13 B. Kudisch, M. Maiuri, L. Moretti, M. B. Oviedo, L. Wang, D. G. Oblinsky, R. K. Prud'homme, B. M. Wong, S. A. McGill and G. D. Scholes, *Proc. Natl. Acad. Sci. U. S. A.*, 2020, **117**, 11289–11298.

14 P. Brumer and M. Shapiro, *Acc. Chem. Res.*, 1989, **22**, 407–413.
15 J. Somlói, V. A. Kazakov and D. J. Tannor, *Chem. Phys.*, 1993, **172**, 85–98.
16 W. Zhu, J. Botina and H. Rabitz, *J. Chem. Phys.*, 1998, **108**, 1953–1963.
17 C. Brif, R. Chakrabarti and H. Rabitz, *New J. Phys.*, 2010, **12**, 075008.
18 M. Abdelhafez, D. I. Schuster and J. Koch, *Phys. Rev. A*, 2019, **99**, 052327.
19 D. J. Tannor, V. Kazakov and V. Orlov, in *Control of Photochemical Branching: Novel Procedures for Finding Optimal Pulses and Global Upper Bounds*, ed. J. Broeckhove and L. Lathouwers, Springer US, Boston, MA, 1992, pp. 347–360.
20 N. Khaneja, T. Reiss, C. Kehlet, T. Schulte-Herbrüggen and S. J. Glaser, *J. Magn. Reson.*, 2005, **172**, 296–305.
21 T. Caneva, T. Calarco and S. Montangero, *Phys. Rev. A: At., Mol., Opt. Phys.*, 2011, **84**, 022326.
22 W. Zhu and H. Rabitz, *J. Chem. Phys.*, 1998, **109**, 385–391.
23 X. Wang, A. Kumar, C. R. Shelton and B. M. Wong, *Phys. Chem. Chem. Phys.*, 2020, **22**, 22889–22899.
24 C. Chen, D. Dong, H.-X. Li, J. Chu and T.-J. Tarn, *IEEE Trans. Neural Netw. Learn. Syst.*, 2013, **25**, 920–933.
25 T. Fösel, P. Tighineanu, T. Weiss and F. Marquardt, *Phys. Rev. X*, 2018, **8**, 031084.
26 X.-M. Zhang, Z. Wei, R. Asad, X.-C. Yang and X. Wang, *Npj Quantum Inf.*, 2019, **5**, 1–7.
27 M. Y. Niu, S. Boixo, V. N. Smelyanskiy and H. Neven, *Npj Quantum Inf.*, 2019, **5**, 1–8.
28 M. Bukov, A. G. Day, D. Sels, P. Weinberg, A. Polkovnikov and P. Mehta, *Phys. Rev. X*, 2018, **8**, 031086.
29 J. Mackeprang, D. B. R. Dasari and J. Wrachtrup, *Quantum Mach. Intell.*, 2020, **2**, 1–14.
30 P. V. D. Hoff, S. Thallmair, M. Kowalewski, R. Siemering and R. D. Vivie-Riedle, *Phys. Chem. Chem. Phys.*, 2012, **14**, 14460–14485.
31 S. Thallmair, D. Keefer, F. Rott and R. de Vivie-Riedle, *J. Phys. B: At., Mol. Opt. Phys.*, 2017, **50**, 082001.
32 T. Brixner and G. Gerber, *ChemPhysChem*, 2003, **4**, 418–438.
33 M. Dantus and V. V. Lozovoy, *Chem. Rev.*, 2004, **104**, 1813–1860.
34 E. B. Wilson, J. C. Decius and P. C. Cross, *Molecular Vibrations: the Theory of Infrared and Raman Vibrational Spectra*, Dover Publications, New York, NY, 1955.
35 K. Fukui, *Acc. Chem. Res.*, 1981, **14**, 363–368.
36 K. Fukui, *J. Phys. Chem.*, 1970, **74**, 4161–4163.
37 B. M. Wong, A. H. Steeves and R. W. Field, *J. Phys. Chem. B*, 2006, **110**, 18912–18920.
38 A. Raza, C. Hong, X. Wang, A. Kumar, C. R. Shelton and B. M. Wong, *Comput. Phys. Commun.*, 2021, **258**, 107541.
39 N. Khaneja, T. Reiss, C. Kehlet, T. Schulte-Herbrüggen and S. J. Glaser, *J. Magn. Reson.*, 2005, **172**, 296–305.
40 QuTiP: Quantum Toolbox in Python, **https://qutip.org/docs/latest/modules/qutip/qobj.html#Qobj.expm**.
41 J. Johansson, P. Nation and F. Nori, *Comput. Phys. Commun.*, 2013, **184**, 1234–1240.
42 H. Gharibnejad, B. Schneider, M. Leadingham and H. Schmale, *Comput. Phys. Commun.*, 2020, **252**, 106808.
43 R. S. Sutton and A. G. Barto, *Reinforcement learning: An introduction*, MIT Press, 2018.
44 A. Paszke, S. Gross, S. Chintala, G. Chanan, E. Yang, Z. DeVito, Z. Lin, A. Desmaison, L. Antiga and A. Lerer, Automatic differentiation in PyTorch, 2017.
45 M. L. Puterman, *Markov decision processes: discrete stochastic dynamic programming*, John Wiley & Sons, 2014.
46 V. Mnih, K. Kavukcuoglu, D. Silver, A. A. Rusu, J. Veness, M. G. Bellemare, A. Graves, M. Riedmiller, A. K. Fidjeland and G. Ostrovski, *et al.*, *Nature*, 2015, **518**, 529–533.
47 T. Haarnoja, A. Zhou, P. Abbeel and S. Levine, *arXiv*, 2018, preprint, arXiv:1801.01290.
48 Z. Wang, T. Schaul, M. Hessel, H. Hasselt, M. Lanctot and N. Freitas, *International conference on machine learning*, 2016, pp. 1995–2003.
49 H. Van Hasselt, A. Guez and D. Silver, *Proceedings of the AAAI conference on artificial intelligence*, 2016.

